Mansoura Journal of Chemistry Vol. 40 (1) June, 2013.

THERMAL DECOMPOSITION KINETICS OF NANO-LEAD OXALATE

Mohamed.N.H.Hamed[*a], N.H.Amin[a], K.H.Raghda[a], M.A. Mousa[b]
[a]Chemistry Department, Faculty of Education, Ain shams University, Roxy 11757, Cairo, Egypt.
[b]Chemistry Department, Faculty of Science, Benha University, Benha, Egypt.
Corresponding author. Tel.: +202 01013845979, +202 228719873 fax: +202 22581243. E-mail address: nasrmohamed584@yahoo.com

(Received: 23/ 5/ 2013)

ABSTRACT

Thermal decomposition of nano-lead oxalate, $Pb(C_2O_4)$ was studied using non-isothermal gravimetric analysis. The decomposition occurs in only one and the final product were characterized by means of X-ray diffraction (XRD), Fourier transform infra-red (FT-IR) and transmission electron microscopy (TEM) techniques. The activation energies of the decomposition process were calculated through different iso–conversional methods. The decomposition data were analyzed using thirty five solid state reaction models. The data are found to be well expressed by the Avrami-Erofe'ev equation with subsequent growth of n = 1. The thermal decomposition rate increased with decreasing the particle size of lead oxalate. The thermodynamic parameters ($\Delta S^{\#}$, $\Delta H^{\#}$ and $\Delta G^{\#}$) were computed and discussed.

Keywords: nanoparticles; lead oxalate; Thermogravimetric analysis; Non-isothermal decomposition kinetics; Kinetic models

1. INTRODUCTION

Nano-structured materials have attracted the attention of researchers not only by their unique chemical and physical properties but also by their potential applications in many fields, which has stimulated the search for new synthetic methods for these materials **(Keating &**

Natan, 2003 and Chen, et al., 2005). These materials consist of small grains with sizes below100 nm. Despite much attention and intensive investigation of the various physical properties in nano-sized systems, there is an obvious lack of information available on their reactivity and transport properties as well as their effect on the kinetic behavior for the thermal decomposition of solid system **(Shui, et al., 2002)**.

Studies on mechanisms and kinetics of reactions involving solid state are challenging and difficult task with complexity resulting from the great variety of factors with diverse effects, e.g. reconstruction of solid state crystal lattice, formation and growth of new crystallization nuclei, diffusion of reaction products, materials heat conductance, static or dynamic character of the environment, layer thickness, specific area and porosity type, amount and distribution of the active centers on solid state surface, etc. **(Vlaev, et al., 2008)**. Metal oxalates are interesting candidates for nano-structured synthesis because these can be transformed to oxide or metals without losing the ordered structure **(Soare, et al., 2006)**. The thermal decomposition processes of metal oxalates are relatively complicated because of the reduction property of $C_2O_4^{2-}$. So their thermal analysis studies are often in attention **(Jun, et al., 2003)**. A review on the thermal decomposition kinetics and mechanisms of some solid oxalates has been given by many authors **(Dollimore, 1987 and L'vov 2001)**.

Based on the above review and due to that the nanoparticles possess a large surface area and a possibility for large driving force for grain growth and diffusion in solid reactions, thus, the main objective of the present work is to synthesize nano-sized lead oxalates and to investigate their thermal decomposition kinetics using TGA technique. The lead oxalate and the thermal decomposition product were characterized using XRD, TEM and FT-IR techniques. In this study, we assess the extent to which the nano-size influences the reaction rate and the reaction paths. For kinetic computations, several methods employing a series of non-isothermal calculation methods were used.

2. EXPERIMENTAL

2.1. Synthesis of PbC_2O_4

All the Chemicals used were of analytical grade. Nano-sized lead (II) oxalate, [Pb (C_2O_4)] was synthesized by both solvothermal and precipitation methods. According to solvothermal method: lead (II)

nitrate $Pb(NO_3)_2$ (2 mmol) was dissolved in mixed solvents composed of 30 ml ethylene glycol (EG) and 10 ml water containing 0.02 M oleylamine (surfactant) to form a homogeneous solution. Stoichiometric amount of potassium oxalate dissolved in an equal volume of identical solution was added dropwise to the above solution under magnetic stirring. The solution was stirred for about 10 min and then transferred into an autoclave, which was then tightly sealed and hydrothermally treated at 100 ^oC for 24 hours in an oven. The product was collected by centrifugation and washed with deionized water and absolute ethanol several times and dried in air at 60^oC **(Niasari, et al., 2009)**. This sample was denoted as S_S.

For precipitation method, high purity $Pb(NO_3)_2$ was used as the source of lead and A.R. oxalic acid was used as the precipitant. Lead nitrate was dissolved in distilled water to prepare an aqueous solution of $0.028 mol\,l^{-1}$. This solution was added into $0.028 mol\,l^{-1}$ solution of oxalic acid dissolved in ethanol under mechanical stirring for 3 min. An ethanol solution was used because metal oxalates have very low solubility in ethanol. The precipitate was filtered, washed several times by ethanol and dried in an oven at 100 ^oC for 48 hours**(Choi, et al., 1994)**. The sample was denoted as S_P.

2.2. Characterization

The thermal decomposition of lead oxalate samples was studied by TGA technique using Shimadzu model TGA-50H. The TG curves of the oxalate were obtained under static air in a temperature range of 25 – 600 ^oC using 5 mg of each sample and heating rates of 5, 10, 15 and 20 °C min^{-1}. Both lead oxalate and lead oxide (final product after heating the lead oxalate at 450^oC) were characterized by FT-IR, XRD and TEM. FT-IR was carried out by KBr pellet technique on a FT-IR spectrophotometer model Jasco FTIR 4100. XRD measurements were performed on a Bruker AXSD8 advance X-ray diffractometer using Cu K_α (λ = 0.15418 nm) radiation. The size and morphology of the samples were detected by TEM electron microscopy model Joel 2010.

3. DECOMPOSITION KINETICS

3.1. Theoretical Approach

Kinetic analysis of heterogeneous thermophysical processes is not only the key factor in following and understanding the investigated

thermal processes, but it has also practical applications such as determining the time–evolution of a sample behavior under other temperature conditions than it has been performed. The complete description of a thermophysical process is done through kinetic triplet parameters $\{E_a, A, f(\alpha)\}$, where E_a is the activation energy, A is the pre-exponential factor, $f(\alpha)$ represents the mathematical form of the mechanism to be assumed for the process and α is the conversion degree. The reaction model may take various forms based on nucleation and nucleus growth, phase boundary reaction, diffusion, and chemical reaction **(Rotaru, et al., 2010)** .

A commonly used rate equation in the non-isothermal decomposition kinetics is

$$\frac{d\alpha}{dt} = k(T) f(\alpha) \quad (1)$$

Where k is the rate constant and the conversion factor α is defined as:

$$\alpha = \frac{(m_i - m_t)}{(m_i - m_\infty)} \quad (2)$$

Where m_i is the initial mass of the sample, m_t is the mass of the sample at time t, m_∞ is the residual mass of the sample at the end of the reaction. Integration of Eq. (1) gives the integral rate law:

$$g(\alpha) = kt \quad (3)$$

The rate constant k is generally given by the Arrhenius equation:

$$k = A \exp(-E_a/RT)$$

Where E_a is the activation energy, R is the gas constant and T is the absolute temperature. The combination of Eqs. (1) and (4) gives the following relationship:

$$d\alpha/dt = A \exp(-E_a/RT)\, f(\alpha) \quad (5)$$

For a dynamic TGA process, introducing the heating rate, β= dT/dt, into Eq. (5), giving Eq. (6):

$$d\alpha/dT = (A/\beta) \exp(-E_a/RT) f(\alpha) \quad (6)$$

The conversion function $f(\alpha)$ for a solid-state reaction depends on the reaction mechanism and according to these mechanisms Eq. (6) can generally be written as:

$$\int_0^\alpha \frac{d\alpha}{\alpha^m (1-\alpha)^n [-\ln(1-\alpha)]^p} = \frac{A}{\beta} \int_0^T \exp\left(-\frac{E_a}{RT}\right) dT \quad (7)$$

Where m, n and p are exponent factors, one of them always being zero **(Šesták & Berggren, 1971)**. The solutions of the left hand side integral depend on the explicit expression of the function f (α) and are denoted as

g (α). The formal expressions of the functions g (α) depend on the conversion mechanism and its mathematical model **(Šesták & Berggren, 1971, Heide, et al., 1975 and Zhang et al., 1999)**. The latter usually represents the limiting stage of the reaction, the chemical reactions; random nucleation and nuclei growth; phase boundary reaction or diffusion. Algebraic expressions of functions of the most common reaction mechanisms operating in solid-state reactions are presented in Table 1 **(Vlaev, et al., 2008: Šesták & Berggren, 1971; Heide et al., 1975; Zhang, et al., 1999 and Liqing & Donghua, 2004)**.

3.2 Calculation of kinetic parameters

3.2.1. Iso-conversional methods

Iso-conversion methods employ multiple temperature programs (e.g., different heating rates) in order to obtain data on varying rates at a constant extent of conversion **(Vlaev et al., 2008, Liqing and Donghua, 2004, Friedman,1964, Ozawa,1965, Flynn and Wall, 1966, Kissinger, 1956, Akahira and Sunose, 1971, Gao et al., 2002, Chunxiu et al., 2004, Popescu,1996, Senum and Yang,1977)**. The correct determination of non-isothermal kinetic parameters involves the use of experimental data recorded at several heating rates. These data have allowed to applying the iso-conversion (model-free) methods in accessing the activation energy on the conversion degree that can be correlated with the investigated process mechanism.

3.2.2. Kinetic parameters using single heating rate:

Table 1 shows the basic model functions usually employed for the kinetic study of solid state reactions. Data from TG and DTG curves in the decomposition range $0.1<\alpha<0.9$ were used to determine the kinetic parameters of the process in all used calculations. The integral method of Coats and Redfern **(Coats & Redfern, 1964)** Eq. (8) and Ŝatava-Šestàk equation **(Ŝkvara & Šestàk, 1975)** Eq. (9): have been applied for determining the kinetic parameters by a single thermoanalytical curve. This method utilizes the asymptotic series expansion for approximating the exponential integral in Eq. (7), giving

$$\ln\left(\frac{g(\alpha)}{T^2}\right) = ln\left[\frac{AR}{\beta E_a}\left(1-\frac{2RT}{E_a}\right)\right] - \frac{E_a}{RT} \cong ln\left(\frac{AR}{\beta E_a}\right) - \frac{E_a}{RT} \quad (8)$$

$$log[g(\alpha)] = log\left(\frac{AE_a}{\beta R}\right) - 2.135 - 0.4567\frac{E_a}{RT} \quad (9)$$

Plotting the left hand sides of Eq. (8) and Eq. (9), which includes $g(\alpha)$ versus $1/T$, gives E_a and A from the slope and intercept respectively. The model that gives the best linear fit is selected as the chosen model.

Table (1): Algebraic expression of functions g (α) and *f* (α) and its corresponding mechanism**.**

Several authors **(Liqing & Donghua, 2004; Madhysudanan, et al., 1986; Madhysudanan, et al., 1993 and Wanjun, et al., 2003)** suggested different solutions of the temperature integral in Eq. (7), sustaining the opinion that this increases the precision of the kinetic parameters being calculated. For instance, Madhusudanan–Krishnan–Ninan **(Madhysudanan, et al., 1986 and Madhysudanan, et al., 1993)** suggested the following equation:

$$\ln\left[\frac{g(\alpha)}{T^{1.921903}}\right] = \left[\frac{\ln AE_a}{\beta R} + 5.772050 - 1.921905\ln E_a\right] - \frac{0.120394E_a}{T} \quad (10)$$

and **Wanjun *et al*. (2003)** suggested the equation:

$$\ln\left(\frac{g(\alpha)}{T^2}\right) = \ln\left[\frac{AR}{\beta\left(1.00198882E_a + 1.87391198RT_p\right)}\right] - \frac{E_a}{RT} \quad (11)$$

Equations (8) – (11) imply that there would be differences in the calculated values of the activation energy and pre-exponential factor A even when the same g (α) function is used. To find which calculation procedure would turn out to be the most suitable, they were estimated by the criterion "the best" correlation coefficient of the linear regression R^2 for Eqs. (8) – (11). The advantage of these equations is that the values of E_a and A can be calculated on the basis of single rate thermogravimetric curves and the type of the most probable mechanism function of the studied reaction can be determined. For the calculations of the kinetic and thermodynamic parameters a computer program was designed for all the data manipulations.

4. RESULTS AND DISCUSSION

4.1. Thermal stability of lead oxalate

TGA curves for thermal decomposition of lead oxalate samples (S_P and S_S) are shown in Figs. 1(a−b). The curves are practically identical, showing only one weight loss step in the temperature range 238–330 °C. The weight loss is about 25 %, which is close to the theoretical value (24.39 wt %). This weight loss is due to the decomposition of lead oxalate to lead oxide because the oxidation number of the lead ions is constant during the thermal decomposition process **(Niasari, et al., 2009)**. Table 2 shows that S_P sample decomposes at lower temperature than that found for S_S with larger particle size (as will be seen later). This refers to that the smaller particle size of lead oxalate is more reactive than that of the bigger one.

Table (2): TGA data for the thermal decomposition of PbC_2O_4 (β = 10 °C min^{-1})

Sample	d_{XRD} (nm)	TG plateau (°C)	Mass loss %
S_S	55	238−330	25 (24.29)
S_P	22	165−360	24.3 (24.29)

( ) calculated mass, %

Fig. 1a

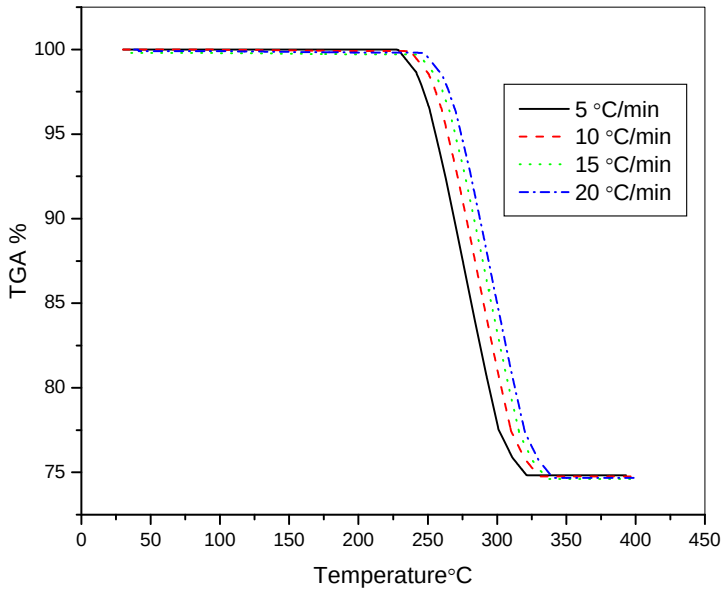

Fig. 1b

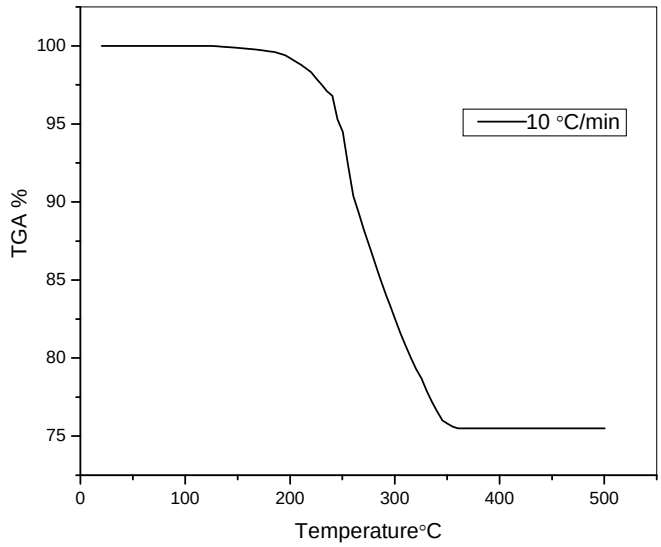

Fig. (1): TG of thermal degradation curves of PbC_2O_4: (a) S_S at different heating rates and (b) TG of S_P at a heating rate of 10 °C/min

4.2. Characterization

Figs. 2(a–d) show XRD for lead oxalate (PbC_2O_4) and lead oxide (PbO) samples. In Figs. 2(a–b), the peaks obtained for both samples (S_p and S_S) coincide with anorthic cell reported for lead oxalate card JCPDS No. 11–0723. The broadening of the peaks for both samples referring to their nanometer sizes. The crystalline sizes are estimated from XRD line broadening using the Debye Scherrer equation **(Klug & Alexander, 1970 and Jenkins & Snyder, 1996)** Eq. (16).

$$d_{XRD} = \frac{0.9\lambda}{\beta \cos\theta} \qquad (16)$$

Where d is the crystallite size, λ is the wave length used in XRD (0.15418 nm), θ is the Bragg angle, and β is the half line width. The average size of S_P and S_S is estimated to be 22 and 55nm, respectively.

The XRD patterns of the decomposition residues (PbO) are shown in Fig. 2(c–d). All the observed diffraction peaks registered at the following 2θ values: 29.2655º, 32.7673 º, 37.9928º, 45.3588º, 51.0335º, 56.2369º, 59.4584º, 60.0836 º, 74.1012 º, 75.8592 º corresponding to the crystal planes (1 0 1), (2 0 0), (2 0 1), (0 2 2), (2 0 2), (3 1 1), (2 2 2), (0 4 0), (3 3 1) and (0 0 4) of the tetragonal lattice of PbO (β-PbO, JCPDS No.

01-0824). The average crystallite size (D_c) for PbO produced from S_P and S_S samples is estimated to be 15 and 35 nm, respectively. This reveals that the synthetic methods reported here can be used for producing nano-sized PbO.

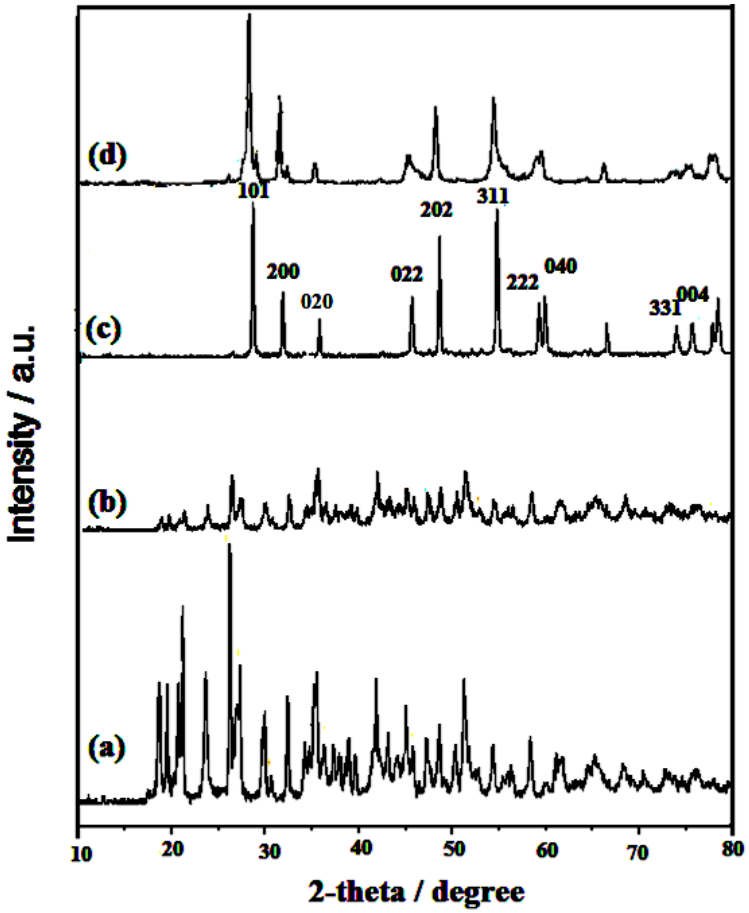

Fig. (2): XRD patterns of PbC_2O_4: S_P (a), S_S (b) and PbO; (c) produced from S_P, (d) produced from S_S

The particle sizes of the studied samples were also investigated using TEM technique, Figs. 3(a–d). Figs. (3a, 3b) exhibit lead oxalate particles with sizes of ~22 and 55 nm for S_p and S_S specimens, respectively. The TEM images in Figs. (3c, 3d) confirm the nano-metric size of the PbO with size of ~15 nm for the oxide produced from S_P sample and 35 nm for that produced from S_S sample. Thus, the difference

obtained in the size of PbO particles implies that the synthesis route of oxalate plays a crucial role in determining the size of oxide particles produced.

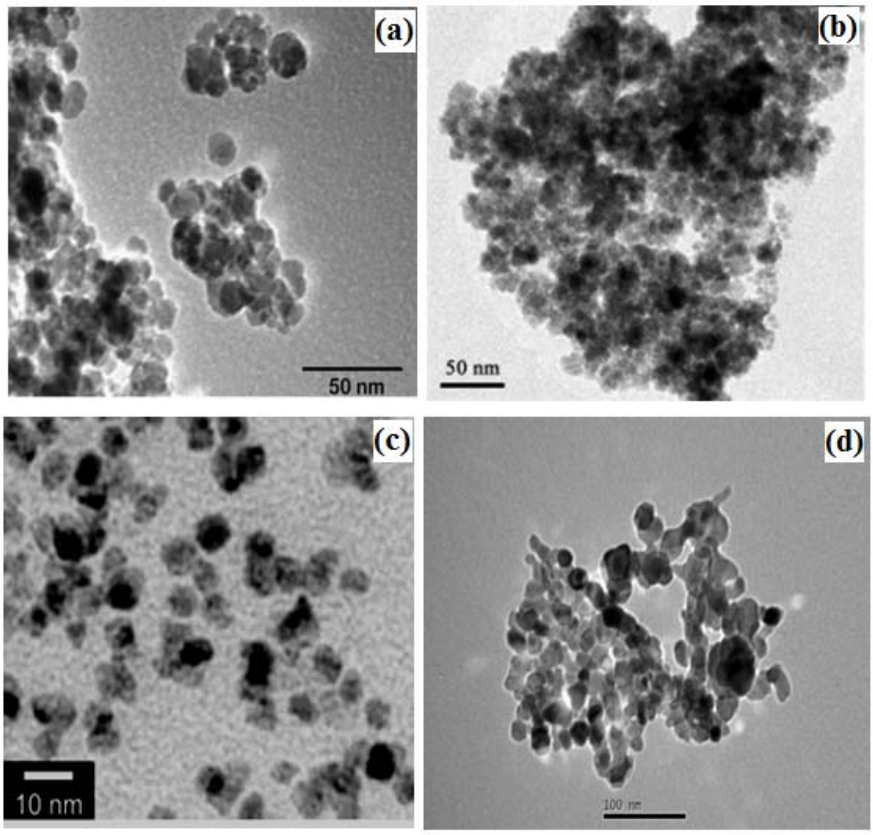

Fig. (3): TEM images of PbC_2O_4: S_P (a), S_S (b) and PbO; (c) produced from S_P, (d) produced from S_S

The FT-IR spectra of lead oxalate and lead oxide samples are shown in Fig. 4. The FT-IR spectra of [Pb (C_2O_4)] shows a very weak absorption band at around 3470 cm^{-1}, suggesting the presence of a small amount of water absorption on the surface of Pb (C_2O_4) after handling. The double absorption peaks that appear at 1645–1662 and 1610–1662 cm^{-1} are due to the asymmetric vibrations of the carbonyl group and the absorption peaks at 1369–1384 and 1287–1290 cm^{-1} are assigned to $\nu_{s(C-O)}+\delta_{(OCO)}$ modes. Two distinct peaks at 759–776 and 481–508 cm^{-1} are attributed to the out–of–plane bending mode of water and O–C–O in-plane bending mode of oxalate, respectively **(Niasari, et al., 2009 and**

Nakamoto, 1991), which indicates the formation of [Pb (O_4C_2)]. The FT-IR spectra of the β-PbO nanocrystals (Figs. 4(c–d)) show a peak at 432–451 cm^{-1}, which is assigned to the Pb–O bond.

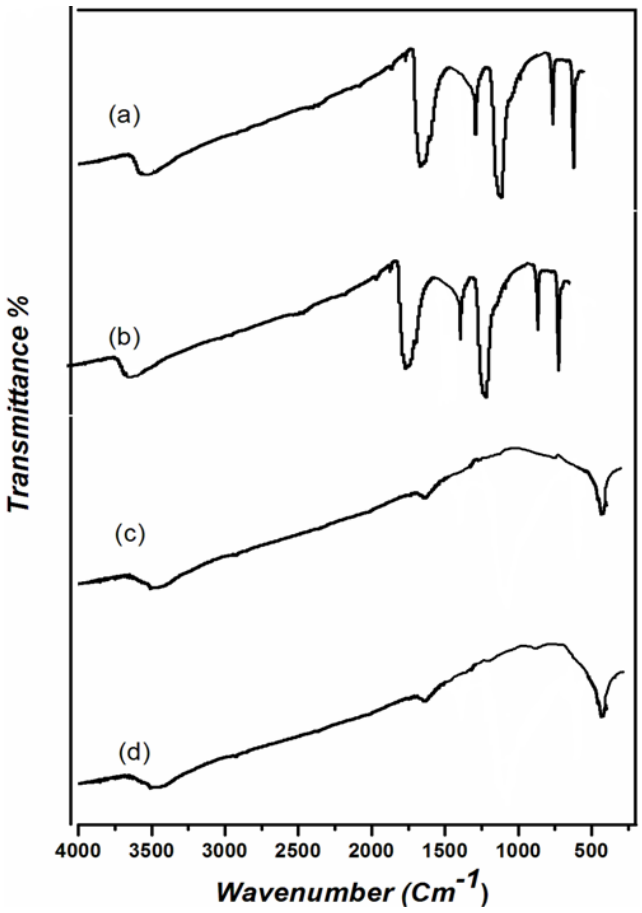

Fig. (4): FT-IR spectra of PbC_2O_4: S_P (a), S_S (b) and PbO; (c) produced from S_P, (d) produced from S_S.

4.3. Kinetics of thermal decomposition

4.3.1. Calculation of activation energy using model free method

The basic data of α and T collected from the TG curves for the thermal decomposition of S_P specimen at various heating rates (5, 10, 15, and 20 °C min^{-1}) are illustrated in Table 3. These data have been used to get the apparent activation energy (E_a) values for the two decomposition stages by applying the iso-conversion (model-free) methods. They were

calculated at fraction conversion 0.1< α <0.9 using each of Flynn–Wall–Ozawa (FWO) (Eq. 13) **(Ozawa, 1965 and Flynn & Wall, 1966)**, Kissinger–Akahira–Sunose (KAS) (Eq. 14) **(Kissinger, 1956 and Akahira & Sunose, 1971)**, Friedman (Eq. 15) [16] and Kissinger (Eq. 16) **(Kissinger, 1956)**:

$$\ln\beta = ln\left(\frac{AE_a}{g(\alpha)R}\right) - 5.3305 - 1.5016\frac{E_a}{RT} \quad (13)$$

$$\ln\frac{\beta}{T^2} = ln\frac{AR}{g(\alpha)E_a} - \frac{E_a}{RT} \quad (14)$$

$$ln\left(\frac{d\alpha}{dt}\right) = ln[Af(\alpha)] - \frac{E_a}{RT} \quad (15)$$

$$\ln\frac{\beta}{T_p^2} = ln\frac{AE_a}{g(\alpha)R} - \frac{E_a}{RT_p} \quad (16)$$

By plotting ln β *vs.* 1/T, ln β/T^2 *vs.* 1/T, ln (dα/dt) *vs.* 1/T and ln β/T_p^2 *vs.* $1/T_p$ and using a linear regressive of least squares method, Figs. 5, 6, 7and 8, the apparent activation energy value (E_a) for the decomposition of PbC_2O_4 at different α values were calculated. The results obtained are listed in Table 4. From which it can be seen that the E_a–values calculated from OFW, KAS and Kissinger methods are close to each other and differ slightly than that found by Friedman.

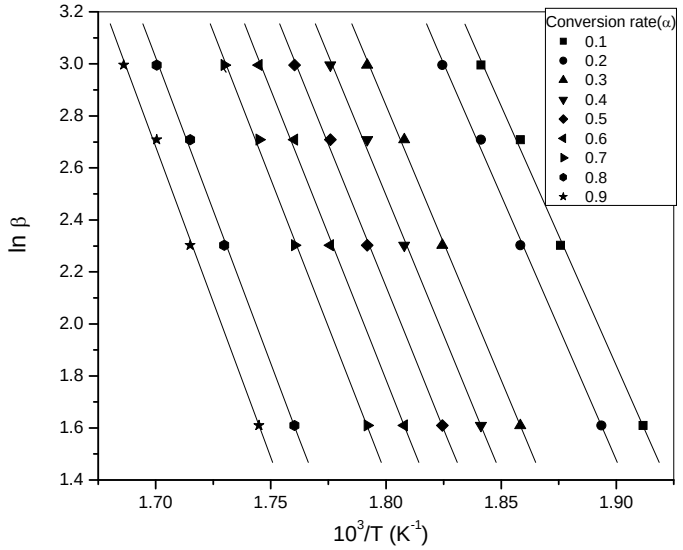

Fig. (5): Iso-conversional plots at various conversion degrees (α) for PbC_2O_4 (S_S), according OFW calculation procedure

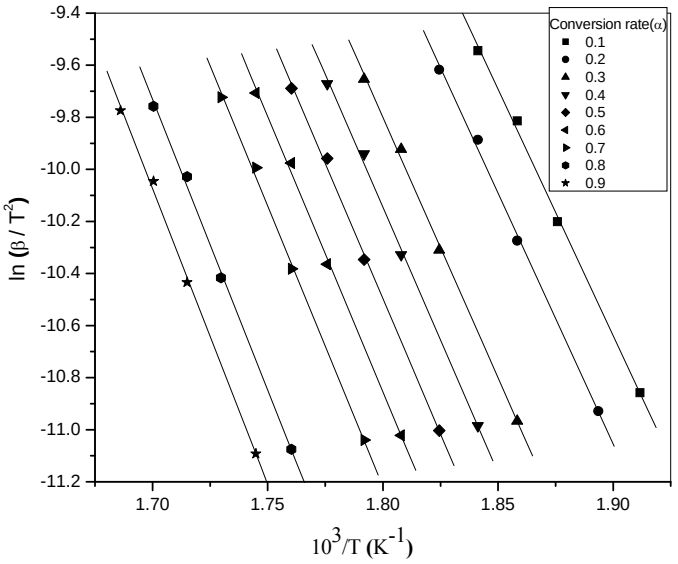

Fig. (6): Iso-conversional plots at various conversion degrees (α) for PbC_2O_4 (S_S), according KAS calculation procedure

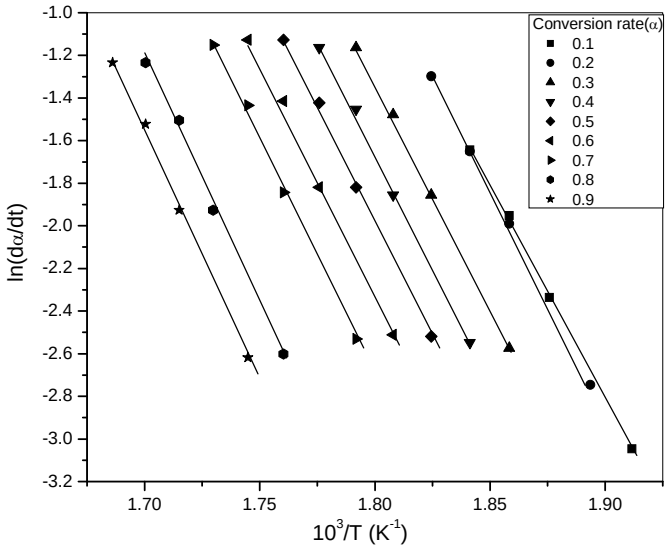

Fig. (7): Iso-conversional plots at various conversion degrees (α) for PbC_2O_4 (S_S), according Friedman calculation procedure

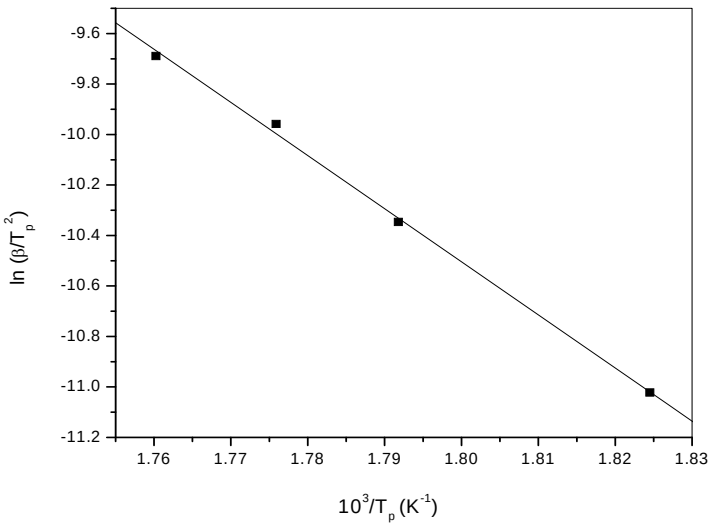

Fig. (8): Iso-conversional plots at various conversion degrees (α) for PbC_2O_4 (S_S), according Kissinger calculation procedure

4.3.2. Calculation of activation energy by iterative procedure

According to Eqs. (13) and (14), the reaction mechanism and the shape of g (α) function have no effect on the obtained activation energy values (E_a). Thus, an iterative procedure was used to get more exact value for activation energy by using the next equations (17, 18):

$$\ln\frac{\beta}{H(x)} = \ln\left(\frac{AE_a}{g(\alpha)R}\right) - 5.3305 - 1.5016\frac{E_a}{RT} \qquad (17)$$

and

$$\ln\frac{\beta}{h(x)T^2} = \ln\frac{AR}{g(\alpha)E_a} - \frac{E_a}{RT} \qquad (18)$$

Because

$$g(\alpha) = \int_0^{\alpha}\frac{d\alpha}{f(\alpha)} \approx \frac{A}{\beta}\int_0^{T} e^{-E_a/RT}dT = \frac{AE_a e^{-x}}{\beta R x^2}h(x) \qquad (19)$$

Where: $h(x)$ is expressed by the fourth Senum and Yang approximation formulae **(Popescu, 1996, Senum and Yang, 1977):**

$$h(x) = \frac{x^4 + 18x^3 + 86x^2 + 96x}{x^4 + 20x^3 + 120x^2 + 240x + 120} \qquad (20)$$

Where $x = E_a/RT$ and H(x) is equal to **(Liqing & Donghua, 2004)**:

$$H(x) = \frac{h(x)x^{-2}\exp(-x)}{0.0048\exp(-1.0516x)} \quad (21)$$

The iterative procedure performed involved the following steps: (i) Assume h(x) = 1 or H(x) = 1 to estimate the initial value of the activation energy E_a. The conventional iso-conversional methods stop the calculation at this step; (ii) using E_{a1}, calculate a new value of E_{a2} for the activation energy from the plot of ln [β/H(x)] vs. 1/T or ln [β/h(x) T^2) vs. 1/T; (iii) repeat step (ii), replacing E_{a1} with E_{a2} .When $E_{a_{it}} - E_{a_{it-1}} \leq 0.1\ kJ\ mol^{-1}$, the last value of $E_{a_{it}}$ was considered to be the exact value of the activation energy of the reaction **(Vlaev, et al., 2008)**.

The activation energy values ($E_{a_{it}}$) obtained using iterative method, through the application of Eqs. (13), (14), (16) and (17) on the decomposition α data given in Table 3, are listed in Table 4. From which it can be seen that each of E_a–values obtained by KAS and OFW for both dehydration and decomposition steps are close to the $E_{a_{it}}$–values obtained by iterative procedure.

Table (3): Thermal decomposition temperature of PbC_2O_4 (S_S) at different conversion degrees (α)

α	**β (K min^{-1})**			
	5	**10**	**15**	**20**
0.1	523.1	533.1	538.1	543.1
0.2	528.1	538.1	543.1	548.1
0.3	538.1	548.1	553.1	558.1
0.4	543.1	553.1	558.1	563.1
0.5	548.1	558.1	563.1	568.1
0.6	553.1	563.1	568.1	573.1
0.7	558.1	568.1	573.1	578.1
0.8	568.1	578.1	583.1	588.1
0.9	573.1	583.1	588.1	593.1

Table (4): Dependence of activation energy E_a (kJ mol^{-1}) on the degree of conversion α using OFW, KAS, Friedman and Kissinger calculation procedures and calculation of activation energy by iterative methods for nano-lead oxalate (S_S) .

α (Degree of conversion)	E_a kJmol^{-1}				$E_{a_{it}}$ (kJmol^{-1}) by iterative methods		A (min^{-1})	
	Friedman	**OFW**	**KAS**	**Kissinger**	**Eq. (14)**	**Eq. (15)**	**Eq. (14)**	**Eq. (15)**
0.1	167.1	157.76	157.04	175	157.76	157.28	1.9E14	1.9E14
0.2	173.9	160.73	160.09		160.31	160.31	5.7E14	5.8E14
0.3	177.2	166.77	166.27		166.49	166.75	1.9E15	2.0E15
0.4	178.3	169.83	169.41		169.63	169.63	3.8E15	3.8E15
0.5	182.2	172.91	172.57		172.8	172.79	7.3E15	7.3E15
0.6	184.9	176.1	175.76		175.99	175.98	1.3E16	1.4E16
0.7	187.6	179.17	178.98		179.21	179.21	2.5E16	2.6E16
0.8	193.2	185.55	185.51		185.62	185.74	6.9E16	6.9E16
0.9	198.1	188.77	188.83		189.05	189.1	1.4E17	1.4E17
Average	182.5	173.06	172.72	175	173	173	2.9E+16	2.92E+16

4.3.3. Determination of the most probable mechanism function

For determining the most probable mechanism, i.e. $g(\alpha)$ function, the values of the conversion α corresponding to multiple rates taken at the same temperature were put into the left side of Eq. (22) **(Vlaev, et al., 2008 and Liqing & Donghua, 2004)** and all different types of mechanism functions, $g(\alpha)$, presented in Table 1 were tested by plotting ln $g(\alpha)$ vs. ln β and using a linear regressive of least squares method.

$$\ln g(\alpha) = \left[\ln\frac{AE_a}{R} + \ln\frac{e^{-x}}{x^2} + \ln h(x)\right] - \ln\beta \qquad (22)$$

If the mechanism studied conforms to certain g (α) function, the slope of the straight line should be close to −1 and the linear correlation coefficient R^2 is higher. The most probable mechanism obtained for the thermal decomposition of the sample investigated is listed in Table 5. From which it can be seen that the random nucleation mechanism (obtained by Avrami-Erofeev) with subsequent growth of n = 1 is the most probable describing function for the PbC_2O_4 decomposition step.

Table (5): The shape of the most probable mechanism function g (α), slope and the correlation Coefficients of linear regression R^2 for nano-lead oxalate (S_S).

Mechanism	**Shape of g(α) Function**	**PbC_2O_4**	
		Slope	R^2
$F_{3/2}$	$\ln\alpha$	-0.776	0.999
F_3	$(1-\alpha)^{-2}-1$	-1.237	0.995
A_1,F_1	$-ln(1-\alpha)$	-1.003	0.999
A_2	$[-ln(1-\alpha)]^{1/2}$	-0.312	0.998

4.3.4. Calculation of kinetic parameters using a single heating rate

The kinetic parameters were also determined using a single heating rate by applying the equations (8) – (11) of Coats and Redfern, Ŝatava−Šestàk, Madhysudanan–Krishnan–Ninan, and Wanjun et al., respectively. The apparent activation energy values (E_a), pre-exponential factor (A) and the most probable reaction mechanism functions were determined. The results obtained are presented in Table 6. From which it can be seen that regardless of the used calculation procedure, the E_a–values are found to decrease with decreasing the particle size [E_a (for sample S_P) < E_a (for sample S_S)]. Also, it can be seen that the kinetic parameters obtained by all methods are close together, except A–value obtained by Ŝatava-Šestàk. Moreover, it should be mentioned here that the activation energy values obtained by the single heating rate agree to some extent with that found by the multi heating rate methods, Table 4.

Table (6): Kinetic parameters obtained with the exponential model (the most probable mechanism function g (α)) for non-isothermal decomposition of PbC_2O_4 samples at a heating rate of 10 °C min^{-1}

Name sample	Heating rate	calculation procedure	Kinetic model g(α)	R^2	E_α (kJ mol^{-1})	A(min^{-1})
S_S	Single (β=10 °C min^{-1})	Coats Redfern	Avrami – Erofeev equation A_1,F_1 (n=1)	0.985 [0.988]	131 [69.1]	6.12E+11 [6.01E+5]
		Wanjun et al	Avrami – Erofeev equation A_1,F_1 (n=1)	0.985 [0.988]	131 [69.1]	6.53E+11 [6.83E+5]
		Madhusudanan-Krishnan-Ninan	Avrami – Erofeev equation A_1,F_1 (n=1)	0.985 [0.988]	132 [69.1]	6.85E+11 [7.11E+5]
		Šatava-Šestàk	Avrami – Erofeev equation A_1,F_1 (n=1)	0.983 [0.988]	310 [171.5]	5.83E+29 [4.13E+15]

[ ] represent data for lead oxalate with smaller particle size (S_p)

4.3.5. Calculation of pre-exponential factor in Arrhenius equation and thermodynamic parameters

The pre-exponential factor A was calculated from the intercept of the plots of $\ln \beta/H(X)$ *vs.* $1/T$ and $\ln \beta/H(x)T^2$ *vs.* $1/T$, Eqs. 17 and 18, respectively, through inserting the most probable g (α) function obtained.

According to the theory of the activated complex (transition state) of Eyring **(Vlaev, et al., 2008; Boonchom & Puttawong, 2010 and Chen et al., 2012)**, the following general equation may be written:

$$A = \frac{ek_B T_p}{h} exp\left(\frac{\Delta S^{\neq}}{R}\right) \quad (23)$$

Where: e = 2.7183 is the Neper number; k_B – Boltzmann constant; h – Plank constant, and T_p is the peak temperature of DTG curve. The change of the activated entropy $\Delta S^{\neq}$ can be calculated according to the formula:

$$\Delta S^{\neq} = R\ln\frac{Ah}{e k_D T_p} \quad (24)$$

Since

$$\Delta H^{\neq} = E_a - RT_p \quad (25)$$

The changes of the enthalpy $\Delta H^{\neq}$ and Gibbs free energy $\Delta G^{\neq}$ for the activated complex can be also calculated by using equation (26):

$$\Delta G^{\neq} = \Delta H^{\neq} - T_p \Delta S^{\neq} \quad (26)$$

The values of $\Delta S^{\neq}$, $\Delta H^{\neq}$ and $\Delta G^{\neq}$ were calculated at $T = T_P$ (T_P is the DTG peak temperature at the corresponding stage), since this temperature characterizes the highest rate of the process, and therefore, it is an important parameter. The results obtained are given in Table 7. From which it can be seen that all the thermodynamic parameters obtained $\Delta S^{\neq}$, $\Delta H^{\neq}$ and $\Delta G^{\neq}$ are positive, indicating that the thermal decomposition is a fast non spontaneous decomposition process and connected with the introduction of heat.

Table (7): Thermodynamic parameters of $\Delta S^{\neq}$, $\Delta H^{\neq}$ and $\Delta G^{\neq}$ for thermal decomposition of PbC_2O_4 (S_s).

Parameters	PbC_2O_4	
	OFW	**KAS**
$\Delta S^{\neq}\ (J\ mol^{-1}K^{-1})$	68.8	68.9
$\Delta H^{\neq}(K\ J\ mol^{-1})$	149.7	149.7
$\Delta G^{\neq}\ (K\ J\ mol^{-1})$	108.1	108.05

5. CONCLUSIONS

The thermal decomposition and the non-isothermal kinetics of the nano-sized PbC_2O_4 were studied under the non-isothermal condition by TG method. The decomposition of lead oxalate occurs in one step with a decrease in the initial decomposition temperature by decreasing the particle size and the final product is nano-sized PbO. The kinetic parameters were obtained from the analysis of the TG curves by different methods using thirty five kinetic models. The results were compared and found that the kinetic parameters change with each of the particle size and the choice of mechanism function. The most possible kinetic model function has been estimated through the multiple linear regression method. The Avrami-Erofeev equation gives the best fit for the measured experimental data. The average activation energy values of the thermal decomposition process obtained by the KAS, FWO, Friedman and Kissinger methods were found to be 177+/- 5$kJmol^{-1}$. The main conclusion is that the decomposition rate of lead oxalate to lead oxide increases with increasing the surface area of the oxalate due to decreasing its particle size.

REFERENCES

Akahira, T., Sunose, T., Sci. Technol. 16 **(1971)** 22–31.

Boonchom, B., Puttawong, S., Physica, B: Condensed Matter 405 **(2010)** 2350–2355.

Chen, F. X., Zhou, C. R., Li, G. P., J. Therm. Anal. Calorim. 109 **(2012)**1457–1462.

Chen, L.J., Zhang, S.M., Wu Z.S., Zhang, Z.J., Dang, H.X., Mater. Lett. 59 **(2005)** 3119–3121.

Choi H.L., Enomoto N., Nakagawa Z.E., Journal of Materials Science 29 **(1994)** 3239–3242.

Chunxiu G., Yufand S., Donghua C., J. Therm. Anal. Cal. 76 **(2004)** 203–216.

Coats A.W., Redfern J.P., Nature (Lond) 201 **(1964)** 68–69.

Dollimore D., Thermochim. Acta 117 **(1987)** 331–363.

Flynn J. H., Wall L. A., Polym. Lett. 4 **(1966)** 323–328.

Friedman H.L., Journal of Polymer Science Part C: Polymer Symposia 6 **(1964)** 183–195.

Gao Z., Amasaki I., Nakada M., Thermochim. Acta 385 **(2002)** 95–103.

Heide K., Höland W., Gölker H., Seyfarth K., Müller B., Sauer R., Thermochim. Acta 13 **(1975)** 365–378.

Jenkins R., Snyder R.L., John Wiley and Sons Inc, New York, **(1996)**, p. 90.

Jun L., Xing Z. F., Wei R. Y., Qian H. Y., Fei N. Y., Thermochimica Acta 406 **(2003)** 77–87.

Keating C.D., Natan M.J., Adv. Mater. 45 **(2003)** 451–454.

Kissinger H. E., J Res Natl Bur Stand, 57 **(1956)** 217–221.

Klug H.P., Alexander L.E., 2nd ed, Wiley, New York, **(1970)**, p. 966.

Liqing L., Donghua C., J Therm Anal Cal. 78 **(2004)** 283–293.

L'vov B.V., Thermochim. Acta 373 **(2001)** 97–124.

Madhysudanan P.M., Krishnan K., Ninan K.N., Thermochim. Acta 221 **(1993)** 13–21.

Madhysudanan P.M., Krishnan K., Ninan K.N., Thermochim. Acta 97 **(1986)** 189–201.

Nakamoto K., Chemical Industry Press, Beijing, **(1991).**

Niasari M. S., Mohandes F., Davar F., Polyhedron 28 **(2009)** 2263–2267.

Ozawa T., Bull. Chem. Soc. Jpn. 38 **(1965)** 1881–1886.

Popescu C., Thermochim. Acta 285 **(1996)** 309–323.

Rotaru A., Constantinescu C., Mândruleanu A., Rotaru P., Moldovan A., Győryová K., Dinescu M., Balek V., Thermochim. Acta 498 **(2010)** 81–91.

Senum G.I., Yang R.T., J. Therm. Anal. 11 **(1977)** 445–447.

Šesták J., Berggren G., Thermochim. Acta 3 **(1971)** 1–12.

Shui M., Yue L., Hua Y., Xu Z., Thermochim. Acta 386 **(2002)** 43–49.

Ŝkvara F., Šestàk J., J. Therm. Anal. Cal. 8 **(1975)** 477–489.

Soare L. C., Bowen P., Lemaitre J., Hofmann H., J. Phys. Chem. B 110 **(2006)** 17763–17771.

Vlaev L., Nedelchev N., Gyurova K., M Zagorcheva., J Anal Appl Pyrolysis 81 **(2008)** 253–262.

Wanjun T., Yuwen L., Hen Z., Zhiyong W., Cunxin W., J. Therm. Anal. Cal. 74 **(2003)** 309–315.

Zhang J.J., Ge L.G., Zha X.L., Dai Y.J., Chen H.L., Mo L.P., J. Therm. Anal. Cal. 58 **(1999)** 269–278.

كيناتيكا التحلل الحرارى لأوكسالات الرصاص النانومترية

محمد نصر *[أ] ، نبيل حفنى[أ] ، رغدة كمال[أ] ، محمود موسى [ب]

[أ] قسم الكيمياء – كلية التربية – جامعة عين شمس

[ب] قسم الكيمياء – كلية العلوم – جامعة بنها

تم دراسة التحلل الحرارى لأوكسالات الرصاص النانومترية بأستخدام جهاز التحليل الحرارى (TGA) تحت الظروف ديناميكية الحرارة. وجد أن التحليل الحرارى تم فى خطوة واحدة حيث تتحول أوكسالات الرصاص الى أكسيد الرصاص نانومترى. وتم تحليل المواد المتفاعلة و الناتجة من التفاعل بأستخدام الأشعة تحت الحمراء، حيود الأشعة السينية والميكروسكوب الألكتروني الماسح والنافذ. كما تم دراسة كيناتيكا تفاعل التحلل بأستخدام خمسه وثلاثون نموذج كيناتيكى. حيث وجد أن التحلل يتم بأستخدام نموذج أفرامى ومعامل تحلل أحادى. وقد تم حساب المعاملات الثرموديناميكية للتفاعل ومناقشة النتائج من حيث تأثير حجم الحبيبات على سرعة التفاعل.